Computation time reducing via non linearity isolating and constraint handling in fixed-point based hierarchical control framework.

Xuan-Huy H Pham, Mazen Alamir, Francois Bonne, Patrick Bonnay

Computation time reducing via non linearity isolating and constraint handling in fixed-point based hierarchical control framework

Xuan-Huy Pham[1,2], Mazen Alamir[1], François Bonne[2] and Patrick Bonnay[2]

***Abstract*— This paper presents an extension of a recently proposed hierarchical control framework applied to a cryogenic system: [1]. Under the assumption made in [1], each subsystem in the decomposition needed at least one control input and one regulated output, which is not practical, especially when a nonlinear subsystem could be decomposed into several smaller subsystems. Consequently, such an assumption limit those valid decompositions that may result in more tractable optimization control problems and thus reduce the computation burden. In this paper, this assumption is removed, allowing greater flexibility in the definition of the decomposition graph, meaning that small nonlinear entities and large linear-considerable subsystems are detached, resulting in more tractable control problems. The impact of this increased flexibility on the computational time and its performance are shown using the same cryogenic station where a decomposition into four subsystems is made possible (instead of two in the previous framework).**

I. Introduction

Decentralized control methods have been an active field, especially when the considered systems are large-scale systems. Generally, this method could be separated into two categories: distributed framework and hierarchical framework. In the former, each subsystem communicates with its neighbors by receiving the other subsystem state and input trajectory in order to update its trajectory throughout many iterations to optimize the centralized cost. Whereas in the latter, the paradigm master-slave is used where the subsystems communicate only with a master (or coordinator) that attempts to coordinate the subsystem behavior to achieve global performance. In [2], the authors have excellently reviewed and proposed a classification of a number of decentralized, distributed, and hierarchical control frameworks. Moreover, the survey book [3] listed more than 35 approaches, which serves as a starting point for developing different techniques.

Recently, a hierarchical control framework has been suggested by [1], in which the system under study is decomposed into a network of interacting subsystems. This framework is structured in two distinct layers. In the lower local layer, each subsystem implements a linear controller in order to regulate a specific output vector. The upper layer consists of a coordinator that exchanges information with the subsystems and optimizes the overall performance by minimizing a global cost through an appropriate set-point vector that is sent to the subsystems (each receives its own set-point vector). In [4], the same framework is validated in the presence of model nonlinearities and in the presence of constraints while using a complexity reduction technique to ensure real-time implementability.

In the two previous works, however, the decomposition of the whole process into a network of subsystems is constrained by the fact that each subsystem is a *controlled system*, i.e., having at least one control input and one or more regulated outputs. Suppose that the large system could be decomposed into several subsystems; among them, ones have control input and output, ones do not have any control input and output. Moreover, the dynamic of these subsystems is influenced by the coupling signal among them. Assuming that nonlinear model predictive controls (NMPCs) are used, the previous decomposition constraint implies that the subsystems without input and output need to be combined with others which has inputs and output, resulting in a new large-scale nonlinear system. Consequently, the high-dimensional NMPC becomes the bottleneck for the overall computation time.

This is the starting point of the present contribution. Indeed, the constraint mentioned above on the decomposition graph is relaxed, making *eligible* decomposition architectures where some of the subsystems show no control or even no regulated output. This enables to use the NMPCs for the particular nonlinear subsystem with a smaller size while considering the coupling influence coming from its neighbors. In addition, the second contribution of this paper is to validate constraint handling properties via local cost by using the proposed hierarchical control framework. Finally, the effectiveness in performance and computation given by relaxing the decomposition constraint will be assessed in this paper.ly

The paper is organized as follows: Section II describes the hierarchical framework investigated in this paper extending the eligibility condition of a decomposition topology. Section III briefly recalls the different steps of the overall hierarchical control. Finally, section IV presents numerical simulation showing the significant advantages that can be obtained thanks to the extension of eligible decomposition topology.

Notation. The following notation is extensively used in the paper. For a sequence of vector $q_{i_1}, q_{i_2}, \dots$, the following notation concatenation operator is used:

$$\bigoplus_{i\in\mathcal{I}} q_i := [q_{i_1}^T, q_{i_2}^T, \dots]^T, \text{ with } \quad i_1 < i_2 < \dots \in \mathcal{I} \qquad (1)$$

Moreover, the bold-faced notation $\boldsymbol{p}$ denotes the profile of a vector variable p over a prediction horizon of length N,

[1]University of Grenoble Alpes, Gipsa-lab,(xuan-huy.pham@grenoble-inp.fr)

[2] University of Grenoble Alpes, IRIG-DSBT, F-38000, Grenoble,France

namely:

$$\boldsymbol{p} = [p^T(k), \ldots, p^T(k+N-1)]^T \in \mathbb{R}^{N \cdot n_p} \tag{2}$$

II. Hierarchical control formulation

In order to better understand the paradigm studied in this contribution, let us consider the situation described in Fig. 1 where a set of interacting subsystems indexed by $\mathcal{N} := \{1, \ldots, n_s\}$ is represented. This set is subdivided into two different subsets:

- The subset of controlled subsystems $\mathcal{N}^{ctr} \subset \mathcal{N}$ having each its control input vector and regulated output vector, denoted by u_s and y_s respectively.
- The complementary subset of subsystems that includes no control input denoted by $N^{unc} := \mathcal{N} - \mathcal{N}^{ctr}$.

Each subsystem S_s sees its dynamics impacted through the so-called coupling signals $v_{s' \to s}$ coming from all subsystems $\{S_{s'}\}_{s' \in \mathcal{N}_s}$ with indices s' that belong to the set of indices $\mathcal{N}_s$ (set of indices of subsystems impacting S_s). Fig. 1 presents the interconnected subsystems at the local layer and the coordinator at the coordination layer. The process between the two layers will be described hereafter.

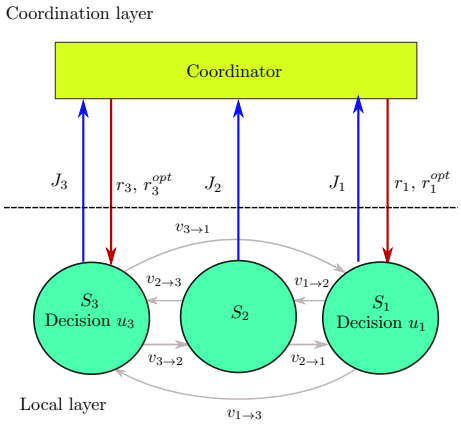

Fig. 1. Example of the hierarchical control architecture and the interconnection network between the subsystems. The presented sets correspond to this example are $\mathcal{N} := \{1,2,3\}$; $\mathcal{N}^{ctr} := \{1,3\}, \mathcal{N}_1 = \{2,3\}, \mathcal{N}_2 = \{1,3\}$, $\mathcal{N}_3 = \{1,2\}$.

Let $\boldsymbol{v}_s^{in}$ and $\boldsymbol{v}_s^{out}$ denote respectively the incoming/outgoing coupling profiles of the subsystem S_s. More precisely:

$$\boldsymbol{v}_s^{in} := \bigoplus_{s' \in \mathcal{N}_s} \boldsymbol{v}_{s' \to s} \quad ; \quad \boldsymbol{v}_s^{out} := \bigoplus_{s' | s \in \mathcal{N}_{s'}} \boldsymbol{v}_{s \to s'} \tag{3}$$

The following assumption is considered regarding the processing that is available locally at the subsystem's level:

Assumption 1: Each subsystem S_s, when given

- a presumed incoming profile $\boldsymbol{v}_s^{in}$ and
- a given individual set-point r_s (required if $s \in \mathcal{N}^{ctr}$),

can process an algorithm to compute what would be:

- Its resulting outgoing profile $\boldsymbol{v}_s^{out}$ and
- Its contribution J_s to the central cost

The central cost is assumed to be of the form:

$$J_c(r, \boldsymbol{v}^{in}) := \sum_{s \in \mathcal{N}^{ctr}} J_s(r_s, \boldsymbol{v}_s^{in}) + \sum_{s \in \mathcal{N}^{unc}} J_s(\boldsymbol{v}_s^{in}) \tag{4}$$

where $r := \bigoplus_{s \in \mathcal{N}^{ctr}} r_s$ and $\boldsymbol{v}^{in} := \bigoplus_{s \in \mathcal{N}} \boldsymbol{v}_s^{in}$

Note that the computation processed at the local subsystem level depend on the current states x_s of each subsystem of which the coordinator is unaware. As a result, each time the coordinator sends $(r, \boldsymbol{v}^{in})$, the subsystems receive the information that enables to construct the corresponding $\boldsymbol{v}^{out}$, namely there is a map (that depends implicitly on the current state of the system):

$$\boldsymbol{v}^{out} = \boldsymbol{g}_{out}(r, \boldsymbol{v}^{in}) \tag{5}$$

Moreover, the elements of the outgoing coupling profile $\boldsymbol{v}^{out}$ are also those of the incoming coupling profile $\boldsymbol{v}^{in}$ but arranged in a different order. Indeed, both $\boldsymbol{v}^{in}$ and $\boldsymbol{v}^{out}$ are composed of all the profiles of the form $\boldsymbol{v}_{s \to s'}$, for $s \in \mathcal{N}_{s'}$. Therefore, there exists a permutation matrix G_{in} such that :

$$\boldsymbol{v}^{in} = G_{in} \cdot \boldsymbol{v}^{out} \tag{6}$$

Injecting (6) in (5) yields:

$$\boldsymbol{v}^{in} = G_{in} \cdot \boldsymbol{g}_{out}(r, \boldsymbol{v}^{in}) \tag{7}$$

Indeed, equation (7) governs the dynamic of the subsystems at the local layer according to the setpoint r. However, the coordinator at the upper layer is obliged not to know this information of the subsystems. This is the **modular privacy preservation requirement** which is made in order to simplify any changes in the local layer when they occur (readers are referred to [1] for more information).

Then, the central optimization problem presents at the coordination layer can be stated:

$$\min_{r, \boldsymbol{v}^{in}} \quad J_c(r, \boldsymbol{v}^{in}) \tag{8}$$

$$\text{subject to} \quad \boldsymbol{v}^{in} = G_{in} \cdot \boldsymbol{g}_{out}(r, \boldsymbol{v}^{in}) \tag{9}$$

As a matter of fact, the true decision variable in the above optimization problem is r since the constrains (9) fully determine $\boldsymbol{v}^{in}$ for any r. The difficulty lies in the fact that the mathematical expression involved in (9) is totally unknown to the coordinator (**modular privacy preservation requirement**). That is the reason why, in order to solve (8), [1] proposed an algorithm based on fixed-point iteration. Briefly, the algorithm could be summarized as below:

During an updating period $[k, k+1]T_s$ with T_s being the sample time, the process occurring between the two layers are separated into two sub-processes, namely:

Estimate the central cost J_c: For a setpoint r given by the coordinator to the subsystem

1) The coordinator starts by sending an initial guess $\boldsymbol{v}_s^{in,(\sigma=0)}$ regarding the incoming profiles,
2) The subsystems compute their control profiles $\boldsymbol{u}_s$ (if any) and the corresponding outgoing coupling profiles $\hat{\boldsymbol{v}}_s^{out,(\sigma)}$,

3) The subsystems send the outgoing coupling profiles $\hat{\boldsymbol{v}}_s^{out,(\sigma)}$ to the coordinator from which the coordinator can constitute the corresponding incoming coupling profiles $\hat{\boldsymbol{v}}_s^{in,(\sigma)}$ based on (6).
4) To ensure the convergence of the iteration, a stabilizing filter is used to update the profile denoted by $\boldsymbol{v}_s^{in,(\sigma+1)}$,
5) The iterations continue until the termination criteria $\epsilon := \max(|\boldsymbol{v}^{in,(\sigma+1)} - \boldsymbol{v}^{in,(\sigma)}|) \leq$ is satisfied. Then, the subsystems compute their local costs J_s and send it to the coordinator. The coordinator can thus compute the the central cost J_c in 8.

Optimize J_c with respect to r: Repeating the process described above for different values of r, the coordinator disposes of a successive clouds of values of the form:

$$\left\{r^{(i)}, J_c(r, \boldsymbol{v}^{in,\star}(r^{(i)}))\right\} \tag{10}$$

That can be used to derive an iterative and modular privacy-preserving solution of the original problem (8)-(9). (see [1], [4] for the detailed description of the derivative-free trust region based optimization process) and gets the sub-optimal solution r^{opt} in terms of the auxiliary reference vector r. These two sub-processes are described in the next section.

III. Recall on the hierarchical control framework

A. Evaluate central cost by using fixed-point iteration:

In this section, the auxiliary set-point r and the current state x_s are assumed to be frozen. The following describes the fixed-point iteration leading to the computation of $J_c(r, \boldsymbol{v}^{in,\star}(r))$ mentioned briefly in the previous section. The coordinator starts with some initial guesses about the incoming coupling profiles:

$$\boldsymbol{v}_s^{in,(\sigma)}, \quad s \in \mathcal{N}, \quad \sigma = 0 \tag{11}$$

These current guesses are sent to the subsystems S_s, $s \in \mathcal{N}$, so that each subsystem can compute the corresponding outgoing coupling profile $\hat{\boldsymbol{v}}_s^{out,(\sigma+1)}$ and sends it to the coordinator, namely:

$$\hat{\boldsymbol{v}}_s^{out,(\sigma+1)} = \boldsymbol{g}_{out}^{(s)}(r, \boldsymbol{v}_s^{in,(\sigma)}) \tag{12}$$

where $\boldsymbol{g}_{out}^{(s)}(\cdot)$ is the function available at subsystem S_s that computes the outgoing coupling profile $\hat{\boldsymbol{v}}_s^{out,(\sigma+1)}$. Note that the value of $\hat{\boldsymbol{v}}_s^{out,(\sigma+1)}$ depends implicitly on the current state at the subsystem S_s.

After receiving these profiles, the coordinator can allocate the elements of the outgoing coupling profile $\hat{\boldsymbol{v}}^{out,(\sigma+1)}$ in the estimate of the incoming coupling profile of each subsystem that is compatible with the received outgoing profiles:

$$\hat{\boldsymbol{v}}_s^{in,(\sigma+1)} = G_{in}^{(s)} \cdot \hat{\boldsymbol{v}}^{out,(\sigma+1)} \tag{13}$$

concatenating these profiles enables to update the total incoming profile $\boldsymbol{v}^{in,(\sigma+1)}$ according to a filtering step:

$$\boldsymbol{v}^{in,(\sigma+1)} = (\mathbb{I} - \Pi) \cdot \boldsymbol{v}^{in,(\sigma)} + \Pi \cdot \hat{\boldsymbol{v}}^{in,(\sigma+1)} \tag{14}$$

where $\mathbb{I}$ is the identity matrix with the appropriate dimension. The matrix Π is an advanced filter that is computed so that the resulting operator is a contraction (for more information about Π, readers are referred to [1]). Then, the coordinator sends $\boldsymbol{v}_s^{in,(\sigma+1)}$ (for $s \in \{1, \ldots, n_s\}$) to the subsystem S_s for the next round.

It is essential to note that the coherence constraints (9) is fulfilled only when the fixed-point iteration converges to some fixed-point $\boldsymbol{v}^{in,(\infty)}$. In practice, the procedure described above is repeated until some termination condition is met. This can be defined by the logical condition

$$\epsilon = \|\boldsymbol{v}^{in,(\sigma+1)} - \boldsymbol{v}^{in,(\sigma)}\| \leq \epsilon_{max} \quad \text{or} \quad \sigma \geq \sigma_{max}$$

After the convergence of the iterations, each subsystem S_s computes the the local cost: $J_s(\cdot)$ and sends it back to coordinator in order to compute the central cost, namely:

$$J_c(r, \boldsymbol{v}^{in,(\infty)}) := \sum_{s \in \mathcal{N}^{ctr}} J_s(r_s, \boldsymbol{v}_s^{in,(\infty)}) + \sum_{s \in \mathcal{N}^{unc}} J_s(\boldsymbol{v}_s^{in,(\infty)}) \tag{15}$$

The detail of the local cost will be described in the section IV-B. The resolution of r_s^{opt}, for $s \in \mathcal{N}^{ctr}$, is described in the next subsection.

B. Optimizing the central cost

The previous section presented an algorithm that is used to evaluate the central cost J_c associated with a given setpoint r. Then, as mentioned in II, the whole process is launched in an updating period $[k, k+1]T_s$ in order to find the optimal setpoint to be sent to the subsystems. To do so, one can use any derivative-free solver (BOBYQA [5], Genetic algorithm [6], see also [7]), which uses the evaluated central cost associated to the setpoint r to find the optimal one. For instance, a method was proposed in [1] to find the optimal setpoint by evaluating each setpoint in a $\mathbf{G}$ grid. This grid is defined in an iteratively updated trust-region built around the previous solution $r^{opt}(k-1)$. By having a map of these setpoints, the coordinator can perform a quadratic approximation, which is solved for the optimal setpoint. This is also the method used in this paper.

Finally, having the optimal setpoint r^{opt} sent from the coordinator, the subsystem S_s, $s \in \mathcal{N}^{ctr}$ compute their decision profiles and applies the first element to the plant.

IV. Simulation-based validation

The objective of this section is to validate the relevance of extending the eligibility of subsystems definition in the decomposition architecture. The plant is first recalled, for which two possible decomposition topologies are defined, where the first exploits the new degrees of freedom while the second respects the previous decomposition condition. Comparison between the results of the two architectures in terms of performance and computation time is made in order to validate the contribution of the paper.

A. Investigated system introduction

The investigated system that is used in order to validate the framework is a cold box of a cryogenic refrigerator. Fig. 2 shows a block diagram of the cold box system consisting of a Joule-Thomson cycle and a Brayton cycle. The Brayton cycle consists of two heat exchangers, which are NEF_2, NEF_{34} and a turbine T_1. The helium flow is cooled down using the cryogenic turbine T_1 to extract thermal energy from the fluid and by exchanging the heat power through a series of heat exchangers (NEF_x). A part of the helium gas is liquefied by the valve CV_{155} through the isenthalpic process. The allowed flow rate M_{out} for this installation is 70 g/s for safety reasons.

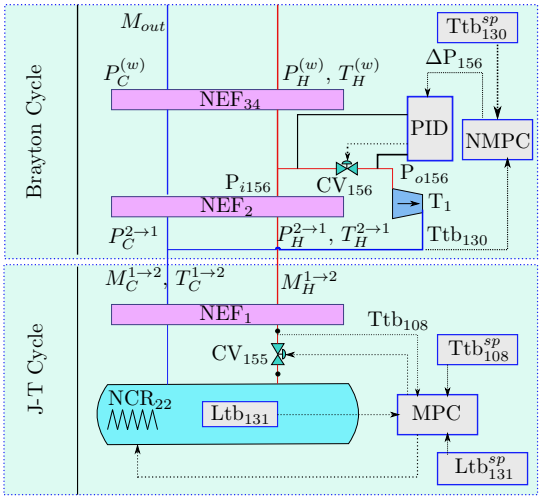

Fig. 2. Block diagram of the cold box plant.

The Manipulated Inputs: There are three control inputs which are CV_{155}, NCR_{22} that are defined below:

1) $\text{CV}_{155} \in [0\%, 100\%]$: This valve is situated at the inlet of the helium bath.
2) $\text{NCR}_{22}^{(a)}$: This heating actuator is located inside the helium bath (S_1). The value of $\text{NCR}_{22}^{(a)}$ is in the range of $[0, 55]$ W. Note that the variable NCR_{22} in Fig. 2 is decomposed into two terms:

$$\text{NCR}_{22} := \text{NCR}_{22}^{(a)} + \text{NCR}_{22}^{(w)} \tag{16}$$

where $\text{NCR}_{22}^{(w)}$ represents the disturbance coming from the heat source.
3) $\Delta\text{P}_{156} \in [0, 12]$ bar: The pressure drop between the inlet pressure and outlet pressure of the valve CV_{156}. It should be noted that the valve CV_{156} is used to control the pressure drop ΔP_{156} between its inlet and outlet pressure. To do so, the local NMPC of the turbine T_1 computes and sends an appropriate value of the pressure drop ΔP_{156} to the PID controller, which acts on the opening position of the valve CV_{156} (Fig. 2).

The Regulated Outputs: There are three regulated outputs (see Figure 2. for the notation):

1) Ltb_{131}: The helium liquid level (%). The set-point is chosen by the operator. In the usual operation, it is set at $\text{Ltb}_{131}^{sp} = 60.5\%$.
2) Ttb_{108}: The temperature at the inlet of the J-T valve must be tightly controlled in order to ensure the efficiency of the liquefaction of the helium.
3) Ttb_{130}: The temperature at the turbine T_1's outlet.

In this contribution, two decomposition topologies of the overall system are compared:

Four-subsystems-decomposition (4ss strategy): The whole system can be seen as a network of four interconnecting subsystems, which are: the Joule-Thomson cycle (S_1), the heat exchanger NEF_2 (S_2), the heat exchanger NEF_{34} (S_3) and the turbine T_1. In this network, the turbine employs a nonlinear model while the heat exchanger models and the Joule-Thomson cycle are linearized around an operating point x_{op}. Note that only the turbine T_1 and Joule-Thomson cycle are controlled by NMPC and MPC, respectively, while the other subsystems are impacted by their decisions. Table I shows the inputs u_s, outputs y_s, and the coupling signal of this topology. Then, the subsystem's state-space representations are listed below:

Subsystem S_1: The Joule-Thomson cycle:

$$x_1^+ = A_1 x_1 + B_1 u_1 + \sum_{s' \in \mathcal{N}_1} G_{s'\to1} v_{s'\to1} + F_1 w_1, \tag{17}$$

$$y_1 = C_1 x_1, \tag{18}$$

$$v_{1\to s'} = C^v_{1\to s'} x_1, \quad s' \in \mathcal{N}_1 \tag{19}$$

where $x_1 \in \mathbb{R}^{30}$ is the state vector of subsystem S_1 and $w_1 = [\text{NCR}_{22}^{(w)}]$ indicates the disturbance vector.

Subsystem S_2 and S_3 : The heat exchangers NEF_2 and NEF_{34}, respectively:

$$x_s^+ = A_s x_s + \sum_{s' \in \mathcal{N}_s} G_{s'\to s} v_{s'\to s} \tag{20}$$

$$y_s = C_s x_s, \quad \text{for } s \in \{2, 3\},\ s' \in \mathcal{N}_s \tag{21}$$

$$v_{s\to s'} = C^v_{s\to s'} x_s \tag{22}$$

where $x_2 \in \mathbb{R}^{34}$ and $x_3 \in \mathbb{R}^{32}$ are the state vectors of subsystem S_2 and S_3, respectively. Note that these two subsystems do not have any control input while their dynamic is affected by other subsystems' decisions through the coupling signal $v_{s'\to s}$. Moreover, the subsystem S_3 has one output which is M_{out}, and because the subsystem S_2 does not have any output, its output equation y_2 does not exist.

Subsystem S_4 : Turbine T_1:

$$y_4 = h_4(u_4, v_4^{in}) \tag{23}$$

$$v_{4\to s'} = g_4(u_4, v_4^{in}), \quad s' \in \mathcal{N}_4 \tag{24}$$

where $v_4^{in} := \bigoplus_{s' \in \mathcal{N}_4} v_{s'\to4}$. Note that the subsystem S_4 is only a static function of control input u_4 and the incoming coupling signal v_4^{in}.

Two-subsystems-decomposition (2ss strategy): This decomposition consists of two subsystems that are the Joule-Thomson cycle (S_1) and the Brayton cycle (S_2) as already depicted in Fig. 2. Note that the turbine T_1 and the two

heat exchangers NEF_2 and NEF_{34} are now combined to become a subsystem S_{234} that represents the Brayton cycle. This subsystem now has one control input and one regulated output, which follows the assumption made in previous work [1]. The model equation of Joule-Thomson cycle is kept unchanged, while the state-space representation of the Brayton cycle can be easily obtained by combining the equations of S_2, S_3 and S_4, namely:

$$x_{234}^{+} = f_{234}(x_{234}, u_4, w_3) \tag{25}$$
$$y_{234} = h_{234}(x_{234}, u_4) \tag{26}$$
$$v_{234\to1} = g_{234}(x_{234}, u_4) \tag{27}$$

where

$$x_{234} = [x_2^T, x_3^T] \quad y_{234} = y_4 \quad v_{234\to1} = [v_{2\to1}] \tag{28}$$

It can be noted that in this new subsystem S_{234}, the non-linearity of the turbine makes the whole model become large-scale nonlinear system despite the fact that the heat exchanger parts are linear.

TABLE I

THE INPUTS, OUTPUTS AND THE COUPLING VARIABLES OF THE 4-SUBSYSTEMS TOPOLOGY. THE NOTATIONS T_C, M_C AND P_C/T_H, M_H AND P_H REPRESENT THE TEMPERATURE, THE FLOW RATE AND THE PRESSURE OF THE COLD/HOT PIPELINE, RESPECTIVELY.

	u_s	y_s	$v_{s\to s'}$
S_1	$\text{NCR}_{22}^{(a)}$ CV_{155}	Ltb_{131} Ttb_{108}	$v_{1\to2} = [M_H^{1\to2}, M_C^{1\to2}, T_C^{1\to2}]^T$
S_2	-	-	$v_{2\to1} = [T_H^{2\to1}, P_H^{2\to1}, P_C^{2\to1}]^T$ $v_{2\to3} = [M_H^{2\to3}, M_C^{2\to3}, T_C^{2\to3}]^T$ $v_{2\to4} = [P_C^{2\to4}]$
S_3	-	M_{out}	$v_{3\to2} = [T_H^{3\to2}, P_H^{3\to2}, P_C^{3\to2}]^T$ $v_{3\to4} = [T_H^{3\to4}, P_H^{3\to4}]^T$
S_4	ΔP_{156}	Ttb_{130}	$v_{4'\to2'} = [M_C^{4\to2}, T_C^{4\to2}]^T$ $v_{4\to3} = [M_H^{4\to3}]$

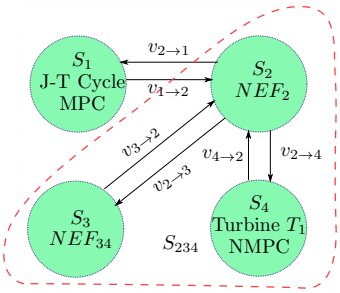

Fig. 3. The interconnection network between the subsystems of the Cold Box.

B. Parameters setting:

The following local costs of each subsystem are defined as below:

For S_1 and S_4 that need to track the desired set-points r_s^d:

$$J_s(r|r_s^d) = \sum_{i=0}^{N-1} \|y_s(k+i) - r_s^d\|^2_{Q_c^{(s)}} + \|u_s(k+i)\|^2_{R_c^{(s)}} \tag{29}$$

where $Q_c^{(s)}$ and $R_c^{(s)}$, for $s \in \{1, 4\}$ are chosen to be positive definite matrices, namely:

$$Q_c^{(1)} = \text{diag}([10^4, 10^4]) \qquad Q_c^{(4)} = 10^4 \tag{30}$$
$$R_c^{(1)} = \text{diag}([0, 0]) \qquad R_c^{(4)} = 0 \tag{31}$$

with diag() denoting a diagonal matrix.

For S_3 that has output M_{out} to be constrained, the constraint violation cost is defined, namely:

$$J_3(r|\overline{y}_3) = \sum_{i=0}^{N-1} \|\max(y_3(k+i) - \overline{y}_3, 0)\|^2_{Q_c^{(3)}} \tag{32}$$

where $\overline{y}_3 = 0.07kg/s$ and $Q_c^{(3)} = 10^{12}$.

Finally, S_2 does not have any contribution to the central cost, its cost is simply defined by $J_2(r) = 0$.

The local costs for the 2-subsystems topology can simply be deduced from the previous choices so that the resulting central cost is identical. In addition, the termination criteria on convergence error ϵ_{max} and the maximum number of iteration described in section III-A are set at $\epsilon_{max} = 10^{-5}$ and $\sigma_{max} = 30$, respectively.

For local controller synthesis, readers are referred to the works in [8], [4]. The system investigated in this simulation is modeled by using the Simulink-based Simcryogenic library [9].

C. Numerical simulation

First, the system behavior using the mentioned strategies are shown in Fig. 4. In this scenario, the system with the hierarchical control is simulated under a disturbance profile $NCR_{22}^{(w)}$(subplot(3,2,5)). Obviously, the 2ss strategy gives better tracking performance on Ttb_{130} (subplot(3,2,3)) since the dynamic of the Brayton cycle is taken into account in the local control problem. Besides, the constraint on M_{out} (subplot(3,2,4)) is satisfied thanks to the constraint penalization cost added in the central. However, it is essential to note that the computation limit is not considered in this simulation, which means the control is applied even though the algorithm can not be finished within the updating period. In addition, Fig. 5 shows the setpoint tracking scenario where the coordinator ensures the constraint satisfaction on M_{out} while proceeding with the setpoint tracking objective.

Second, Fig. 6 shows that the computation time of 4-subsystems topology is significantly shorter than the computation time of the 2-subsystems topology since the large-scale problem optimization control problem of S_2 (2-subsystems topology) is decomposed into more tractable ones.

V. CONCLUSION

In this paper, a hierarchical control method has been applied to a generic case with multiple subsystems. Specifically, the previous assumption made in [1] is removed, allowing for a more flexible decomposition, which gives better performance in terms of computation time and control quality. It is also shown that this hierarchical control method has the ability to take into account subsystem constraints by defining the corresponding local costs. Promising results

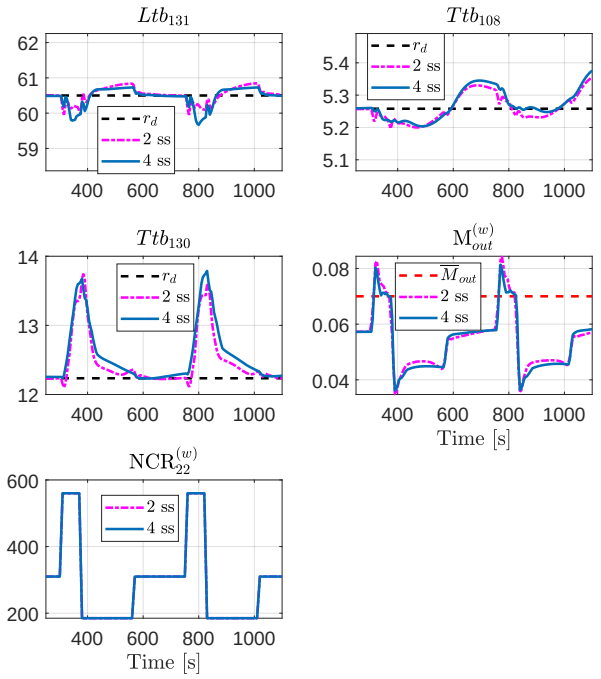

Fig. 4. Comparison of the output behavior between two strategies using hierarchical control where r^d indicates the desired setpoint. Thanks to constraint penalization cost on M_{out}, the coordinator drives the system in a way such that M_{out} satisfies the constraint. Obviously, the Ttb_{130} in the 2ss strategy is better tracking the desired setpoint. However, it is essential to note that in this simulation, the computation time limit is not considered, which means the control is updated even that the computation time exceeds the updating period.

have been obtained with models from the Simcryogenics library on a MATLAB simulation.

Ongoing work aims to validate the control structure, including verifying this approach with a full cryogenic facility (more subsystems) and replacing the filter in (14) with a residual-based iterative method so that the coordinator completely ignores knowledge of the subsystem mathematical equations. The application of machine learning to replace the local layer controllers is also considered.

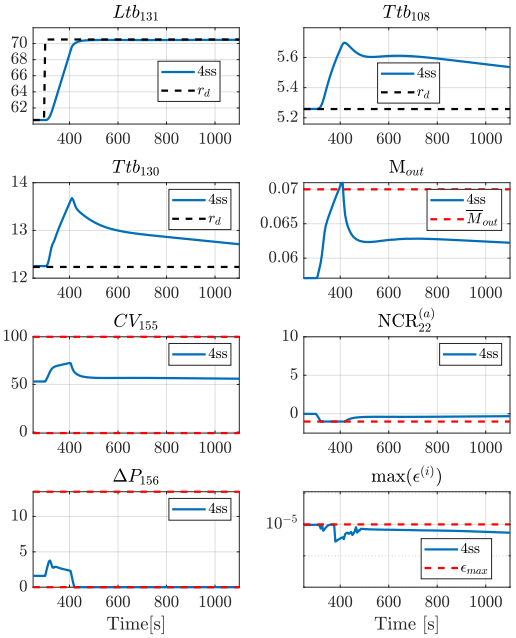

Fig. 5. The system behavior under the hierarchical control framework. In this scenario, the set-point of liquid helium level Ltb_{131} is changed at instant $t = 300$. This figures also shows the actuator behaviors in subplot(4,2,5), subplot(4,2,6) and subplot(4,2,7). Subplot(4,2,8) shows the maximum convergence error of fixed-point iterations $\max(\epsilon^{(i)})$ founded in the grid $\mathcal{G}$ of candidate setpoints at each time step.

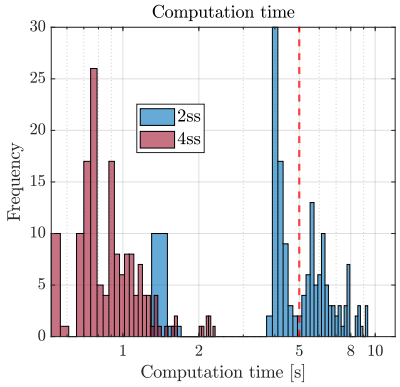

Fig. 6. The computation time of the NMPC in the two strategies. Note that red dash line depicts the sampling time which is $T_s = 5$ seconds. The local MPC problems are synthesized and solved by using Casadi [10] and solver Ipopt, respectively.

REFERENCES

[1] M. Alamir, P. Bonnay, F. Bonne, and V.-V. Trinh, "Fixed-point based hierarchical MPC control design for a cryogenic refrigerator," *Journal of Process Control*, vol. 58, pp. 117–130, 2017.

[2] R. Scattolini, "Architectures for distributed and hierarchical model predictive control – a review," *Journal of Process Control*, vol. 19, no. 5, pp. 723 – 731, 2009.

[3] R. R. Negenborn and J. M. Maestre, *On 35 Approaches for Distributed MPC Made Easy*. Dordrecht: Springer Netherlands, 2014, pp. 1–37.

[4] X.-H. Pham, M. Alamir, F. Bonne, and P. Bonnay, "Revisiting a fixed-point hierarchical control design for cryogenic refrigerators under constraints, nonlinearities and real-time considerations," *European Journal of Control*, vol. 63, pp. 82–96, 2022.

[5] M. J. Powell, "The bobyqa algorithm for bound constrained optimization without derivatives," *Cambridge NA Report NA2009/06, University of Cambridge, Cambridge*, vol. 26, 2009.

[6] S. M. Thede, "An introduction to genetic algorithms," *Journal of Computing Sciences in Colleges*, vol. 20, no. 1, pp. 115–123, 2004.

[7] C. Cartis, J. Fiala, B. Marteau, and L. Roberts, "Improving the flexibility and robustness of model-based derivative-free optimization solvers," *ACM Transactions on Numerical Software*, 2019.

[8] F. Bonne, "Modélisation et contrôle des grands réfrigérateurs cryogéniques," Theses, Université de Grenoble, Dec. 2014. [Online]. Available: https://tel.archives-ouvertes.fr/tel-01133432

[9] F. Bonne, S. Varin, A. Vassal, P. Bonnay, C. Hoa, F. Millet, and J.-M. Poncet, "Simcryogenics: a library to simulate and optimize cryoplant and cryodistribution dynamics," *IOP Conference Series: Materials Science and Engineering*, vol. 755, p. 012076, jun 2020.

[10] J. Andersson, J. Gillis, G. Horn, J. Rawlings, and M. Diehl, "Casadi: a software framework for nonlinear optimization and optimal control," *Mathematical Programming Computation*, vol. 11, pp. 1–36, 2019.